Magnetization of hard superconductor samples subjected to oblique fields

Debjani Karmakar and K. V. Bhagwat
Technical Physics and Prototype Engineering Division, Bhabha Atomic Research Centre, Bombay 400 085, India
(Received 13 March 2001; revised manuscript received 10 July 2001; published 19 December 2001)

The Critical State model (CSM) is examined for infinite cylindrical samples of a hard type-II superconductor subjected to a transverse oblique magnetic field. Our solution is based on a generalization of a result for the surface current density on a cylindrical surface that produces a uniform interior magnetic field. We give arguments that lead to this generalization. This result has enabled us to get an analytical formulation of the CSM, for cylinders of arbitrary cross section, in the form of an infinite system of first order nonlinear differential equations. An important new outcome of the application of an oblique field is that the current densities $\pm J_c$ within the sample are separated not by a line along the applied field direction as one would naively expect, but along a curve that substantially deviates from it. Following an approximation procedure, we obtain the virgin magnetization curves for a superconducting elliptical cylinder for different orientations of the applied magnetic field. Hysteresis loops for parallel and perpendicular components of magnetization are presented for the applied field orientation of 15°.

DOI: 10.1103/PhysRevB.65.024518 PACS number(s): 74.25.Ha, 75.60.Ej

I. INTRODUCTION

The Critical State model (CSM) proposed by Bean[1] is extensively used to analyze magnetization data on hard type-II superconductors. The early solutions due to Bean himself pertained to samples in parallel geometry—an infinite slab and an infinite circular cylinder. Many extensions and generalizations of the CSM have been studied in the literature. Solving the CSM for sample shapes with nonzero demagnetization factor has proved to be a difficult and nontrivial exercise.[2–7] For determining ac losses from superconducting wires there have been some early attempts to obtain flux-fronts numerically.[8–10] In an experimental study, superconductor samples are usually employed with the applied field $\mathbf{B}_a$ along a symmetry direction. Consequently, theoretical studies in the literature invariably assume that $\mathbf{B}_a$ is along a sample symmetry-axis, and this is also taken to be one of the coordinate axes. In all these cases the magnetization is anti-parallel to the applied field. In a realistic sample, magnetization would acquire a perpendicular component due to inherent anisotropy of the material as well as due to sample shape. Even in an isotropic specimen there is a possibility of a misorientation between the direction of $\mathbf{B}_a$ and the sample symmetry axis. A theoretical investigation of samples subjected to oblique fields would be helpful in estimating the geometric contribution[11] to the perpendicular magnetization in both the cases. We are thus led to examine the CSM for samples subjected to an external magnetic field in an oblique direction. Our solution is based on the idea that a given volume current distribution can be broken into infinitesimal shells and that each current shell can be considered as a surface current density.[12] We restrict to cylindrical samples in a transverse geometry because the required expression for the surface current density producing uniform interior field can be easily obtained from our earlier result.[13]

The paper is organized as follows. We begin the next section with a generalization of our result on surface current density producing uniform transverse interior field. Essentially, we develop an expression for surface current density that produces magnetic field in an oblique direction. We then present an analytical formulation of CSM for cylindrical samples in the form of an infinite system of nonlinear ordinary differential equations. Subsequently an approximation method is envisaged. As an illustration, this is worked out for an elliptic cylindrical sample and the results for virgin magnetization curves for different orientations of the field are presented. We also give the hysteresis curves for different reversal fields both for the parallel and the perpendicular components of the sample magnetization. The saturation magnetization and the field for full penetration are obtained as a function of the angle of orientation of the field and are compared with the respective quantities resulting from a model current distribution. For comparing the relative magnitudes of parallel and perpendicular components of saturation magnetization and to check its dependence on sample asymmetry about the field orientation, a sample with a larger aspect ratio has been analyzed. The last section summarizes these results with a discussion.

II. THE SURFACE CURRENT DENSITY

For a cylindrical conductor the surface current density along the z-axis producing uniform transverse interior field B_0 along x-direction is given by[13]

$$\mu_0 J_s = 2\gamma B_0 \sin\phi/|f'(\phi)|. \tag{1}$$

Here ϕ is the angle between the direction of the field B_0 and the vector representing the location of the current density, and $\zeta = f(u)$ represents the conformal mapping that maps the exterior of the boundary $\mathcal{L}$ of the cross-section of the cylinder under consideration to the exterior of a unit circle. The parameter γ stands for the limit of $f(u)/u$ as $u \to \infty$. The quantity $|f'(\phi)|$ is to be understood as the derivative of $f(u)$ evaluated at $u = \exp(\imath\phi)$. In Ref. 13 the parameter γ was assumed to be real. If γ is complex, say, $\gamma = p\exp(\imath\beta)$, then the above formula gets modified and the current density has the form

$$\mu_0 J_s = 2pB_0 \sin(\phi+\beta)/|f'(\phi)|.$$

Now let α be the angle between the direction of B_0, the transverse magnetic field produced by the current density and the *x*-axis. Resolving the field into its *x* and *y* components, viz., $B_{0x}=B_0\cos\alpha$ and $B_{0y}=B_0\sin\alpha$, we see that the net current density can be obtained as a superposition of appropriate current densities resulting from the repeated application of Eq. (1). Since both flow in the same direction they will simply add up and we get

$$\begin{aligned}\mu_0 J_s &= 2pB_0[\cos\alpha\sin(\phi+\beta)-\sin\alpha\cos(\phi+\beta)]/|f'(\phi)| \\ &= 2pB_0\sin(\phi+\beta-\alpha)/|f'(\phi)| \end{aligned} \quad (2)$$

as the surface current density producing uniform transverse interior field along the direction inclined at an angle α to the x-axis. The above result can also be derived from first principles by following the procedure outlined in Ref. 13.

III. FORMULATION OF CSM FOR CYLINDERS

A. Current density, current shells, and flux-fronts

Let us consider a zero field cooled cylindrical sample subjected to a uniform transverse field. As per the CSM the sample responds to changes in the external field by setting up an induced current density J_c starting from the surface. The extent of penetration of flux as well as that of induced current density in the sample is limited by the flux-front. In other words, during the virgin curve, in the region interior to the flux-front both $\mathbf{B}=\mathbf{0}$ and $\mathbf{J}=\mathbf{0}$. In this region the field generated by induced currents exactly cancels the applied field. The field B_a may be reached by sequentially applying a large number infinitesimally small steps of δB_a, starting from zero field. At each of these steps δB_a a new (infinitesimally small) current shell would be set up within the sample generating field in its interior that exactly annuls the change δB_a. An infinitesimal current shell may be viewed as a surface current. Thus the shielding volume current density can be broken up into an effective succession of surface currents. Since each of these current shells (or the equivalent surface current density) generates uniform interior field, it must have the general form given above.

A given flux-front would be characterized by B_a, the magnitude of the applied field. Thus, flux-fronts form a one parameter family of surfaces. At zero field, the flux-front coincides with the sample surface. As B_a is increased monotonically the volume enclosed by the flux-front shrinks in size and more flux penetrates the sample. Eventually at some field $\mathbf{B}_p$ the flux completely penetrates the sample. The magnitude of $\mathbf{B}_p$ depends on the critical current density J_c and sample dimensions, and is deduced from the solution of the model. We shall use the symbol h to denote the flux-front parameter. Consequently, the sample surface corresponds to $h=0$, and the innermost flux-front would be identified by $h=h_a=B_a/\mu_0 J_c b$, where b is one of the semi-axes of the elliptical cross-section of the cylinder.

B. Description of flux-fronts by their conformal map

For analytical description of the family of flux-fronts we conceive of a one to one correspondence between members of the family of flux-fronts and a family of conformal mappings characterized by the parameter h. We require that the conformal mapping associated with a given flux-front map it onto a unit circle and its *exterior* onto the *exterior* of the same unit circle. Let the cross-section of the cylinder be in the ζ-plane ($\zeta=x+\imath y$). For symmetric samples, the family of conformal mappings can be represented by the following series:

$$\zeta = f(u,h) = \sum_{n=1}^{\infty} a_n u^{-(2n-3)}, \quad (3)$$

where the coefficients $\{a_n, n=1,2,\ldots\}$ are in general complex functions of the (real) parameter h. These will be chosen in the form $a_n = p_n \exp(\imath\alpha_n)$. Clearly, if we set $u=\exp(\imath\phi)$, $(-\pi\leqslant\phi<\pi)$, Eq. (3) provides an analytical representation of the flux-front. The initial values of these coefficients viz., $a_1(0)$, $a_2(0)$, $a_3(0)$, ... etc. are obtained by determining the initial conformal mapping of the exterior of the boundary $\mathcal{L}$ of the cross-section of the cylinder onto the exterior of a unit circle. These coefficients evolve as functions of h. The solution consists in obtaining the evolution of the coefficients . The magnetization of the sample is expressible in terms of these coefficients and hence can be obtained.

C. Division of current carrying region into current shells

We have seen that the current carrying region of the sample can be the build up of several infinitesimal current shells, thereby enabling us to view volume current density as a succession of surface current density. We will now explicitly accomplish this by studying the expression for the field generated by the given current density. Let us consider a slightly more general situation when the cylindrical sample carries a (volume) current density $\mathbf{J}(x',y')$ parallel to the axis of the cylinder. As in Ref. 13 we obtain the field $\mathbf{B}_J$ generated by $\mathbf{J}$ from a complex function $B(\zeta)$ defined as

$$B_J(\zeta) = \frac{\mu_0}{2\pi}\int\int \frac{J(x',y')}{\zeta-\zeta'}dx'\,dy', \quad (4)$$

where $\zeta=x+\imath y$ and $\zeta'=x'+\imath y'$. The components of $\mathbf{B}_J$ are obtained as $\mathbf{B}_{Jx}=\Im B_J(\zeta)$ and $\mathbf{B}_{Jy}=\Re B_J(\zeta)$. Effecting a change of variables from $(x',\ y')$ to $(h,\ u'=\exp(\imath\phi')$ by writing $\zeta'=f(u',h)$, where the function f is as defined in Eq. (3). The integral in Eq. (4) can be expressed in the form

$$B(\zeta) = \frac{\mu_0}{2\pi}\int dh \int \frac{J(x',y')}{(\zeta-\zeta')}\frac{|\chi(h,\phi')|}{|f'(h,u')|}ds'. \quad (5)$$

Here $\chi(h,\phi')\equiv x'_h y'_{\phi'} - x'_{\phi'} y'_h$ is the Jacobean of transformation and $ds'=|d\zeta'|=|f'(h,u')|d\phi'$. The net $B(\zeta)$ is clearly seen as produced by a succession of current shells of thickness dh. Each current shell carries a surface current density $J_s=J|\chi|/|f'(h,u')|dh$. Since this surface current density produces uniform interior field, canceling the change δB_a in

the applied field, it should have the same form as in Eq. (2) (with B_0 replaced by $\delta B_0 = -\delta B_a$). This condition leads to the relation

$$\mu_0 J\, dh = 2\,\delta B_0 p_1 \sin(\phi + \alpha_1 - \alpha)/|\chi|. \tag{6}$$

D. Determination of the conformal maps

To determine the conformal maps that consistently provide the evolution of flux-fronts from the sample surface, we choose $\mu_0 J_c b\, dh = \delta B_0 = -\delta B_a$, in Eq. (6) and set $|J| = J_c$ as implied by the CSM. This leads to the equation $|\chi| = 2p_1 b|\sin(\phi+\alpha_1-\alpha)|$. We choose $\chi = 2p_1 b|\sin(\phi+\alpha_1 - \alpha)|$ which is consistent with the above equation and also consistent with the explicit expression for χ derived below. To get this expression we return to Eq. (3) and use the explicit form $a_n = p_n \exp(\imath\alpha_n)$. Separating into real and imaginary parts, gives the transformation equations for x and y in terms of h and ϕ. Using these equations we obtain the required partial derivatives and subsequently get the expression for χ. The foregoing condition provides the starting point to determine the evolution of flux-fronts. Carrying out some simplifications and rearrangement of terms in the expression for χ we cast it as a Fourier series

$$\chi(h,\phi) \equiv \sum_{k=0}^{\infty} \{U_k \cos 2k\phi + V_k \sin 2k\phi\}, \tag{7}$$

where

$$\begin{aligned} U_k = & \sum_{m=1}^{\infty} (2m+2k-3) p_{m+k} \\ & \times \{p_m \alpha'_m \sin(\alpha_m - \alpha_{m+k}) - p'_m \cos(\alpha_m - \alpha_{m+k})\} \\ & + \sum_{m=k+1}^{\infty} (2m-2k-3) p_{m-k} \{p_m \alpha'_m \sin(\alpha_m - \alpha_{m-k}) \\ & - p'_m \cos(\alpha_m - \alpha_{m-k})\}, \end{aligned}$$

$$\begin{aligned} V_k = & \sum_{m=1}^{\infty} (2m+2k-3) p_{m+k} \\ & \times \{p_m \alpha'_m \cos(\alpha_m - \alpha_{m+k}) + p'_m \sin(\alpha_m - \alpha_{m+k})\} \\ & - \sum_{m=k+1}^{\infty} (2m-2k-3) p_{m-k} \{p_m \alpha'_m \cos(\alpha_m - \alpha_{m-k}) \\ & + p'_m \sin(\alpha_m - \alpha_{m-k})\}. \end{aligned}$$

In the above equations the prime on p_m and α_m denotes derivative with respect to h. We also have the Fourier series expansion

$$|\sin(\phi+\alpha_1-\alpha)| \equiv \frac{2}{\pi} - \sum_{k=1}^{\infty} \frac{4}{\pi(4k^2-1)} \cos 2k(\phi+\alpha_1-\alpha). \tag{8}$$

As noted earlier, the condition $|J| = J_c$ implies equality of left hand sides of Eqs. (7) and (8). Hence their right hand sides must also be equal. A comparison of the coefficients of $\cos 2k\phi$ and $\sin 2k\phi$ for $k = 0,1,2,3,\ldots$, appearing on the right hand sides of Eqs. (7) and (8) we get a system of ordinary differential equations for p_n and α_n. The equations can be expressed in a compact form as a system of two matrix equations:

$$\mathbf{A}\mathbf{p}' + \mathbf{B}\mathbf{q} = \mathbf{c}, \tag{9}$$

$$\mathbf{C}\mathbf{p}' + \mathbf{D}\mathbf{q} = \mathbf{d}. \tag{10}$$

Here $\mathbf{p}$, $\mathbf{q}$ are column vectors with elements p_n and $q_n = p_n \alpha'_n$, respectively, and the column vectors $\mathbf{c}$ and $\mathbf{d}$ have elements $c_k = -8p_1 b \cos 2k(\alpha-\alpha_1)/[\pi(4k^2-1)]$ and $d_k = -8p_1 b \sin 2k(\alpha-\alpha_1)/[\pi(4k^2-1)]$. The elements of the matrices $\mathbf{A}$, $\mathbf{B}$, $\mathbf{C}$, and $\mathbf{D}$ are functions of p_n and α_n and can be obtained as

$$\begin{aligned} A_{km} = & -(2m+2k-3) p_{m+k} \cos(\alpha_m - \alpha_{m+k}) \\ & -(2m-2k-3) p_{m-k} \cos(\alpha_m - \alpha_{m-k}) \Theta(m-k), \end{aligned}$$

$$\begin{aligned} B_{km} = & (2m+2k-3) p_{m+k} \sin(\alpha_m - \alpha_{m+k}) \\ & +(2m-2k-3) p_{m-k} \sin(\alpha_m - \alpha_{m-k}) \Theta(m-k), \end{aligned}$$

$$\begin{aligned} C_{km} = & (2m+2k-3) p_{m+k} \sin(\alpha_m - \alpha_{m+k}) \\ & -(2m-2k-3) p_{m-k} \sin(\alpha_m - \alpha_{m-k}) \Theta(m-k), \end{aligned}$$

$$\begin{aligned} D_{km} = & (2m+2k-3) p_{m+k} \cos(\alpha_m - \alpha_{m+k}) \\ & -(2m-2k-3) p_{m-k} \cos(\alpha_m - \alpha_{m-k}) \Theta(m-k), \end{aligned}$$

where the function $\Theta(m-k) = 0$, for $m \leqslant k$, and $= 1$ otherwise . Equations (9) and (10) can be formally solved to obtain the derivatives $\mathbf{p}'$ and $\boldsymbol{\alpha}'$, however, possibility of an exact solution appears very remote. A numerical solution can be obtained by approximating the infinite dimensional matrices by truncation and performing numerical integration of the differential equations. We will now calculate virgin magnetization in terms of the coefficients.

IV. MAGNETIZATION CURVES

A. Virgin magnetization

The magnetization associated with a cylindrical current distribution is given by

$$\mathbf{m}_v = (1/2A) \int\int (\mathbf{r}' \times \mathbf{J}) dx'\, dy', \tag{11}$$

where A is the cross-sectional area of the sample. Changing the variables of integration to (h, ϕ'), noting that the current density is along z-axis and using Eq. (6), we get

$$\mathbf{m}_v = (H^*/A) \int_0^{h_a} \int_{-\pi}^{\pi} p_1 \sin(\phi' - \alpha)(\hat{\mathbf{i}} y' - \hat{\mathbf{j}} x') dh\, d\phi', \tag{12}$$

where $H^* = \mu_0 J_c b$ and $h_a = B_a/H^*$. In this case the cross-sectional area $A = \pi a b$. Carrying out the integration we get the components of magnetization as

$$\mu_0 m_{vx} = (\pi H^*/A) \int_0^{h_a} p_1 \{ p_1 \cos(\alpha) - p_2 \cos(\alpha_2 - \alpha + \alpha_1) \} dh, \quad (13)$$

$$\mu_0 m_{vy} = (\pi H^*/A) \int_0^{h_a} p_1 \{ p_1 \sin(\alpha) - p_2 \sin(\alpha_2 - \alpha + \alpha_1) \} dh. \quad (14)$$

We determined the set of points $x_0(h_a)$ and $y_0(h_a)$ for a fixed value of the parametric angle, say $\phi = 0$ on the flux-contour labeled by h_a. Full penetration field $B_a = H^* h_a$ is determined as the smallest simultaneous zero of $x_0(h_a)$ and $y_0(h_a)$. For $\alpha = 0°$, $y_0(h_a) \equiv 0$ and its intersection with $x_0(h_a)$ is obtained by extrapolation of the latter.

B. Hysteresis loops

A hysteresis loop can be obtained by following the virgin curve upto some field $B_a = B_m$ and then reversing the field direction to reach the field $-B_m$. To complete the loop we carry out another field reversal to reach the field B_m. When the direction of the change in field is reversed at the applied field value B_m, shielding currents in a certain region near the surface also reverse direction. Thus the magnetization $\mathbf{m}\downarrow(B_m - h)$ can be obtained as a superposition $\mathbf{m}\downarrow(B_m - h) = \mathbf{m}_v(B_m, J_c) - \mathbf{m}_v(h, 2J_c)$.

Finally, when the direction of the field change is reversed once again, the magnetization during the field increasing part of the cycle is obtained as $\mathbf{m}\uparrow(B_a) = -\mathbf{m}\downarrow(-B_a)$.

V. RESULTS AND DISCUSSION

We have obtained a general expression for the surface current density producing uniform transverse interior field in an oblique direction. This result is used to study the problem of flux penetration in a cylindrical sample of a hard superconductor subjected to a transverse oblique magnetic field. The formulation leads to an infinite system of nonlinear first order ordinary differential equations (9),(10). We have solved these differential equations numerically, and determined the values of p_n's and α_n's for a set of values of B_a starting from zero value upto $B_a = B_p$, the field for full penetration. The number of coefficients retained in the present calculation is 14. We found that retaining a larger number does not significantly alter final results. We can then construct the various flux-contours as the field penetrates the sample at a definite angle of orientation α with a sample symmetry axis. We have presented in Fig. 1 flux-contours for three different α values for the elliptic cylindrical sample 1(a = 0.4, b = 1.0). It is seen in Fig. 1 that the flux-contours all have a notch (apex). The apex leaves the sample surface as the applied field is increased. The result that apex leaves the sample surface is in general agreement with other numerical calculations for the case $\alpha = 0$ and this feature has also been justified on physical grounds.[12,14]

Apex represents the point on a flux-contour where **J** vanishes. Figure 2 depicts the movement of the apex for different α values. The movement, in general, is along a path

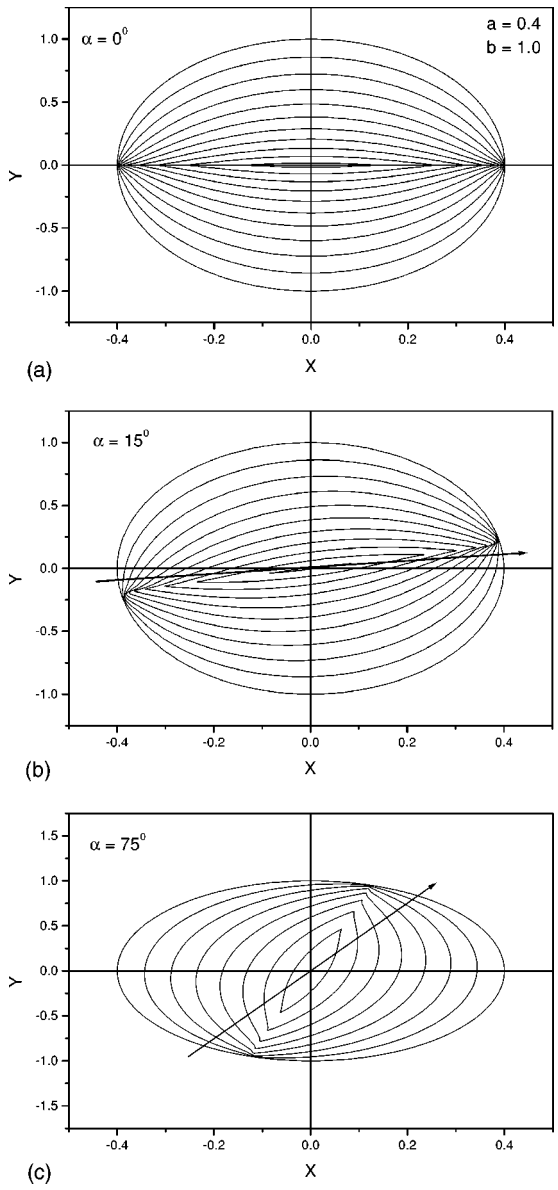

FIG. 1. Flux-contours for an elliptic cylindrical sample with the semi-axes $a = 0.4$ and $b = 1.0$ are shown. The outermost curve corresponds to the sample surface ($\mathbf{B}_a = 0$). Successive contours correspond to a change $\delta \mathbf{B}_a = 0.042 H^*$. Results are shown for three orientions of the applied magnetic field (a) $\alpha = 0°$, (b) $\alpha = 15°$, (c) $\alpha = 75°$ measured from the x-axis. The arrowheaded line in the figures shows the direction of the applied field.

curved near the sample surface and is almost linear otherwise. The curve generated by the movement of the apex as the field penetrates the sample divides the current carrying region into ones carrying the current density $+J_c$ and $-J_c$. In the case of an elliptical cylinder for $\alpha = 0°$ and 90° and for a circular cylinder for all α values, the apex moves along a straight line parallel to the field direction. The linear portion of the curve is, in general, not parallel to the applied field. The angle between the two, however, progressively decreases as the field orientation approaches 90°.

At first sight the result presented in Fig. 2 appears contradictory to what one would expect from asymptotic consider-

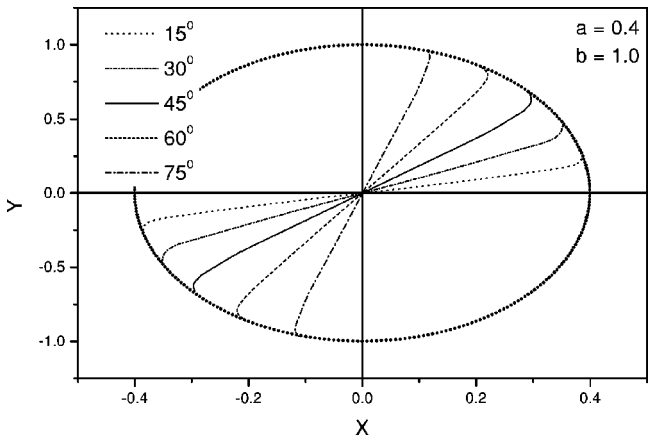

FIG. 2. Movement of the ''apex'' of various flux-fronts for different orientions of the applied field. For the field direction α the apex follows a curved path, the linear portion of which has a slope different from α.

ations. At very high applied fields (beyond the field for full penetration), the whole of sample carries shielding currents and an increase in the external field does not lead to setting up of additional currents. At this stage one would imagine that the change $\delta\mathbf{B}$ in the local field is equal to the change $\delta\mathbf{B_a}$ in the applied field. Thus, if $\mathbf{B}_a$ is increased at a constant rate, it gives rise to an electric field $\mathbf{E}$ that vanishes along the direction of $\mathbf{B}_a$. Since current must flow in the direction of $\mathbf{E}$, $\mathbf{E}=\mathbf{0}$ line must also represent the line of separation between the current densities $\pm J_c$. It is to be noted, however, that before full penetration it is not the electric field accompanying $\delta\mathbf{B_a}$ alone, that governs apex movement. One must also consider a contribution coming from the $\delta\mathbf{B_J}$ generated by the induced currents. A straightforward but detailed calculation reveals that the local electric field due to $\delta\mathbf{B_J}$ generated by the current density (already set up) contains a term that exactly cancels that coming from the change $\delta\mathbf{B_a}$. The resulting $\mathbf{E}$ leads to the apex movement depicted in Fig. 2.

All along the process of field penetration, $\mathbf{B_a}$ is assumed to change *quasi-statically*. Thus beyond full penetration an increase $\delta\mathbf{B}_a$ would generate a surface current density to shield the interior from the change. The surface current density would relax into a current shell (volume current density), the net current density would now exceed the critical current density J_c. The relaxation would then continue by transferring the excess current on the next current shell and the process would continue until the excess current is transferred on to the innermost current shell. Once the change $\delta\mathbf{B}_a$ has been established all over the sample, $\mathbf{J}$ in the innermost shell that is in excess of J_c would start decaying. The direction of $\mathbf{E}$ in the shells external to the innermost shell does not change during the decay of $\mathbf{J}$ leaving the current distribution there unchanged.

The extent of proximity of the slope of the linear portion of the apex movement curve and that of the applied field direction depends on the inherent sample asymmetry about the applied field direction. The more asymmetric the sample the more is the deviation of the above-mentioned slope from the applied field direction.

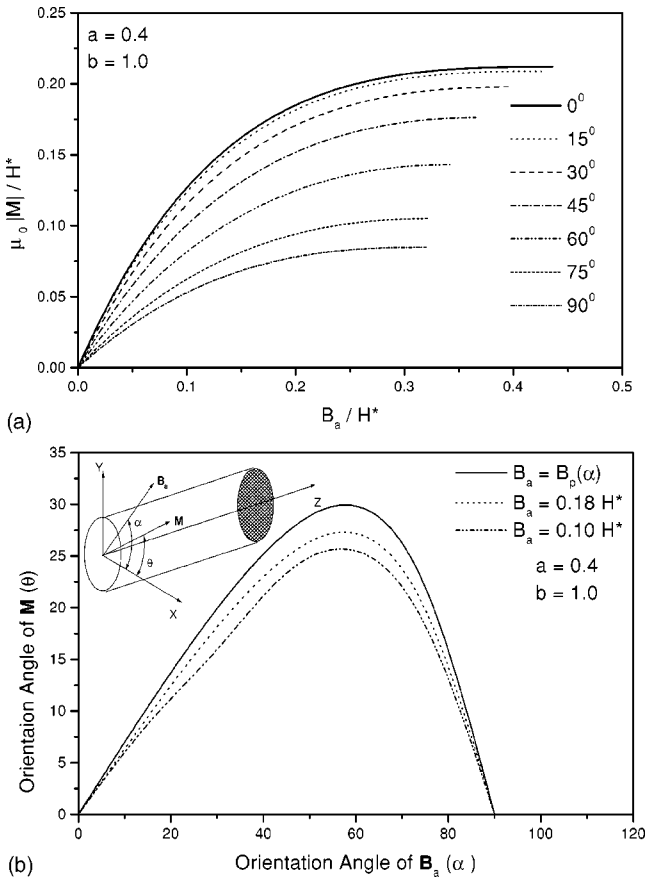

FIG. 3. (a) The virgin magnetization curves for different orientations of the applied magnetic field are shown for $B_a \leqslant B_p$, the field corresponding to full penetration. The elliptical sample has semi-axes $a=0.4$ and $b=1$. (b) Orientation angle θ of $\mathbf{M}$ as a function of the orientation angle α of the applied field is shown for different $\mathbf{B}_a$ values. The inset shows the sample geometry. The orientations of $\mathbf{M}$ and $\mathbf{B}_a$ with respect to the coordinate axes are shown.

In Fig. 3(a) the virgin magnetization curves for different angles of field orientation are plotted for sample 1. The values of saturation magnetization ($M_{\rm sat}$) and B_p vary between the maximum for 0° and minimum for 90°. At each stage of field penetration, we have checked that the field, generated by the induced current distribution, everywhere within the flux-contour indeed cancels the applied field. The direction of the magnetization is, however, different from that of the applied field, implying the existence of a perpendicular component to magnetization. In Fig. 3(b) we have plotted the orientation angle θ of $\mathbf{M}$ as a function of the orientation angle α of the applied field $\mathbf{B}_a$ for two fixed field values as well as at the saturation field B_p. The geometry of the sample is shown as an inset. Figure 3(b) compares well with Fig. 5 of Ref. 11.

To get an estimate of the order of magnitude of these quantities, we considered a model current distribution as $\pm J_c$ on either side of a line through the center, parallel to the applied field and evaluated expressions for saturation magnetization $\underline{M}_{\rm sat}$ and the corresponding field $\underline{B}_p$. As expected, for $\alpha=0°,90°$ the results obtained from the model

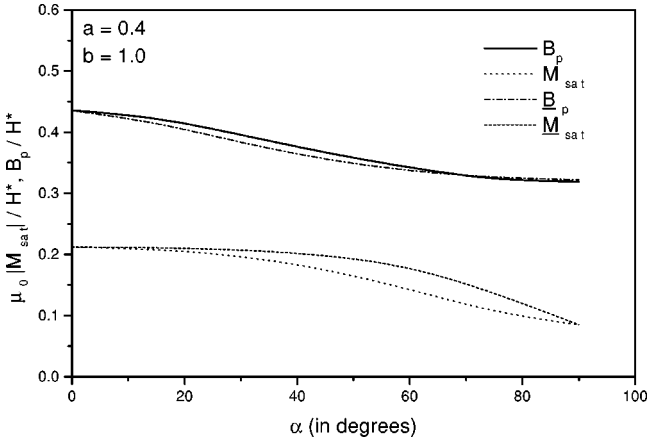

FIG. 4. The variation of saturation magnetization $M_{\rm sat}$ and the field for full penetration B_p, as a function of α is shown. We have also plotted the quantities $\underline{B}_p$ and $\underline{M}_{\rm sat}$ as a function of α for a model current distribution, (see text).

current distribution coincide with exact results (obtained by our numerical procedure). For intermediate values of α the model current distribution leads to results close to the exact results. It is clear, however, that the true values of $M_{\rm sat}$ and B_p depend on the detailed description of field-penetration. Further, as per the model calculation, the directions of both $\underline{B}_p$ and $\underline{M}_{\rm sat}$ are not along the applied field direction. We have shown the angle dependence of B_p, $M_{\rm sat}$, $\underline{B}_p$, and $\underline{M}_{\rm sat}$ in Fig. 4. The mismatch between the model and the exact values of these quantities is apparent. The true separation between the regions carrying $\pm J_c$ at full penetration is depicted in Fig. 2.

We have also presented a set of hysteresis loops for the orientation angle $\alpha = 15°$ for different reversal fields. In Fig. 5(a) we have shown the loops for the parallel component of magnetizaion, while in Fig. 5(b) we have depicted the perpendicular component. These show the familiar behavior well-known for case of $\alpha = 0°$. We may mention in passing that the hysteresis loop for the perpendicular component are unimportant as far as the ac loss is concerned. This is entirely governed by the parallel component.

To get a comparison of the effect of inherent sample asymmetry about the applied field direction we have plotted in Fig. 6 the flux-contours for $\alpha = 75°$ for sample 2 (a = 0.05, b = 1.0). A comparison with Fig. 1(c) shows the difference in the angular position of the point where the apex leaves the sample surface (89.2° for sample 2 and 83.5° for sample 1). This angle can be calculated by noting that the pole of the current density on the sample surface is at the parametric angle $\phi = \alpha$. For an elliptic cylinder the corresponding polar angle, $\theta = \arctan\{(b/a)\tan\alpha\}$. Thus it is clear that the deviation of the path of the apex from the applied field direction is more for more asymmetric samples. We have compared the ratio $(M_\perp / M_\parallel)$ of saturation magnetizations for perpendicular and parallel components for the same angle α. This turns out to be ≈ 0.468 for sample 1 and ≈ 2.503 for sample 2, indicating a relatively larger value for the perpendicular component of magnetizaion for the second sample.

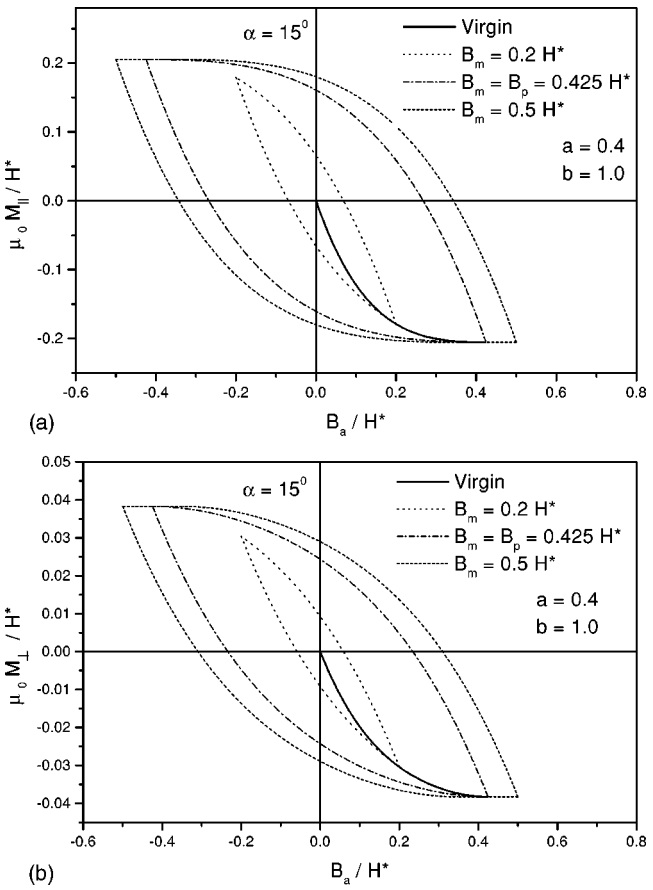

FIG. 5. Virgin curve and Hysteresis loops in the (a) $\mathbf{M}_\parallel$ and (b) $\mathbf{M}_\perp$ components of sample magnetization are shown for various reversal fields. The elliptic cylinder has semi-axes $a = 0.4$ and $b = 1$.

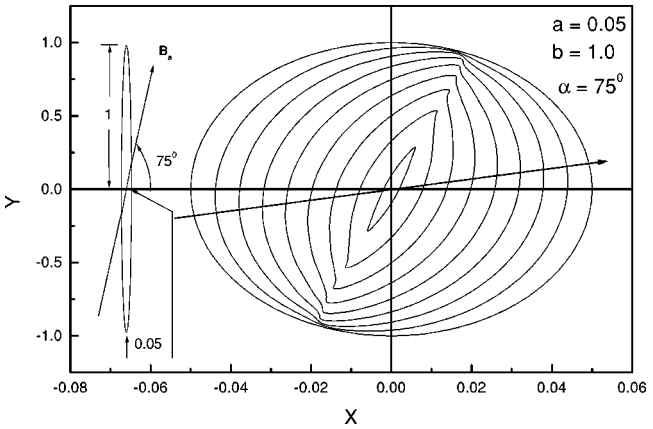

FIG. 6. Flux-contours for the field orientation $\alpha = 75°$ are shown for a sample with semi axes $a = 0.05$ and $b = 1$. The outermost is the sample surface ($\mathbf{B}_a = 0$), successive flux-fronts correspond to a change $\delta\mathbf{B}_a = 0.006H^*$. The shift in the orientations of the flux-contours compared to the earlier sample may be noted. The direction of $\mathbf{B}_a$ is shown by an arrowheaded line. The dimensions of the cross-section of the real sample and the field orientation with respect to the sample symmetry axis are qualitatively shown in the inset.

Finally, we have found that for the samples analyzed in this paper, a misorientation of up to 5° about the direction of the thinner dimension ''a'' does not lead to any significant corrections for the quantities B_p and $M_{\rm sat}$. However, there is a significant change in the magnetization if the misorientation is about the direction of the thicker dimension ''b.'' Lastly, we must emphasize that although we have considered only cylindrical samples of elliptical cross-section, the method presented is applicable to cylinders of arbitrary cross-section.

ACKNOWLEDGMENT

The authors are grateful to Dr. G. Ravikumar for discussions and for providing some earlier references.

[1] C. P. Bean, Rev. Mod. Phys. **36**, 31 (1964).
[2] K. V. Bhagwat and P. Chaddah, Physica C **190**, 444 (1992); *ibid.* **224**, 155 (1994); *ibid.* **280**, 52 (1997).
[3] R. Navarro and L. J. Campbell, Phys. Rev. B **44**, 10 146 (1991).
[4] K. L. Telchow and L. S. Koo, Phys. Rev. B **50**, 6923 (1994).
[5] L. Prigozhin, J. Comput. Phys. **129**, 190 (1996).
[6] J. Mc Donald and J. R. Clem, Phys. Rev. B **53**, 8643 (1996), and references therein.
[7] E. H. Brandt, Phys. Rev. B **54**, 4246 (1996).
[8] M. Ashkin, J. Appl. Phys. **50**, 1760 (1979).
[9] V. B. Zenkevich, V. V. Zheltov, and A. S. Romanyuk, Dokl. Akad. Nauk. SSSR **251**, 339 (1980) [Sov. Phys. Dokl. **25**, 210 (1980)].
[10] J. W. Carr, *AC Loss and Macroscopic Theory of Superconductors* (Gordon & Breach, New York, 1980).
[11] Th. Wolf, A.-C. Bornarel, H. Kupfer, R. Meier-Hirmer, and B. Obst, Phys. Rev. B **56**, 6308 (1997).
[12] K. V. Bhagwat and D. Karmakar, Pramana, J. Phys. **57**, 763 (2001).
[13] K. V. Bhagwat and D. Karmakar, Europhys. Lett. **49**, 715 (2000).
[14] Yu. E. Kuzovlev, JETP Lett. **61**, 1000 (1995).